Available online at www.sciencedirect.com
SCIENCE DIRECT®
Remote Sensing of Environment 90 (2004) 477–489
Remote Sensing of Environment
www.elsevier.com/locate/rse

Land cover characterization of Temperate East Asia using multi-temporal VEGETATION sensor data

Stephen H. Boles[a,*], Xiangming Xiao[a], Jiyuan Liu[b], Qingyuan Zhang[a], Sharav Munkhtuya[c], Siqing Chen[b], Dennis Ojima[d]

[a] *University of New Hampshire, Institute for the Study of Earth, Oceans and Space, Durham, NH 03824, USA*
[b] *Institute of Geographical Sciences and Natural Resources, Chinese Academy of Sciences, Beijing, China*
[c] *National Remote Sensing Center, Ministry of Nature and Environment, Ulaanbaatar, Mongolia*
[d] *Natural Resource Ecology Laboratory, Colorado State University, Fort Collins, CO, USA*

Received 26 August 2003; received in revised form 27 January 2004; accepted 31 January 2004

Abstract

Temperate East Asia (TEA) is characterized by diverse land cover types, including forest and agricultural lands, one of the world's largest temperate grasslands, and extensive desert and barren landscapes. In this paper, we explored the potential of SPOT-4 VEGETATION (VGT) data for the classification of land cover types in TEA. An unsupervised classification was performed using multi-temporal (March–November 2000) VGT-derived spectral indices (Land Surface Water Index [LSWI] and Enhanced Vegetation Index [EVI]) to generate a land cover map of TEA (called *VGT-TEA*). Land cover classes from VGT-TEA were aggregated to broad, general class types, and then compared and validated with classifications derived from fine-resolution (Landsat) data. VGT-TEA produced reasonable results when compared to the Landsat products. Analysis of the seasonal dynamics of LSWI and EVI allows for the identification of distinct growth patterns between different vegetation types. We suggest that LSWI seasonal curves can be used to define the growing season for temperate deciduous vegetation, including grassland types. Seasonal curves of EVI tend to have a slightly greater dynamic range than LSWI during the peak growing season and can be useful in discriminating between vegetation types. By using these two complementary spectral indices, VGT data can be used to produce timely and detailed land cover and phenology maps with limited ancillary data needed.

Keywords: Temperate East Asia; VEGETATION sensor data; Land cover

1. Introduction

Information on land cover status at the regional scale is needed for natural resource management, carbon cycle studies, and modeling of biogeochemistry, hydrology, and climate. Satellite-based remote sensing products can meet these data needs in a timely and consistent manner. Numerous studies of large-scale mapping of land cover have used data from the Advanced Very High Resolution Radiometer (AVHRR; Defries & Townshend, 1994; Loveland et al., 2000). However, the AVHRR sensors, originally designed for meteorological applications, have only two spectral bands (red and near-infrared) that can be used to generate spectral indices of vegetation vigor. Recently, a new generation of optical sensors designed for terrestrial applications has been launched. These include the VEGETATION (VGT) sensor onboard the SPOT-4 satellite and the Moderate Resolution Imaging Spectroradiometer (MODIS) onboard the Terra and Aqua satellites. VGT and MODIS have a number of advantages over AVHRR, including more spectral bands that can be used for vegetation analyses (see Section 2.1 for more details about the VGT sensor). Multi-temporal VGT data have been used to characterize forests in northeastern China (Xiao et al., 2002b) and cropland in southern China (Xiao et al., 2002a). The Global Land Cover program (GLC2000) is an on-going effort to provide a harmonized global land cover product from VGT data using a hierarchical classification scheme. Preliminary results from northern Eurasia are promising (Bartalev et al., 2003); however, only the Russian forest cover has been tested for accuracy, with an R^2 of 0.93 existing between GLC2000 forest areas and official Russian forest statistics (Bartalev et al., 2003).

* Corresponding author. Tel.: +1-603-862-2639; fax: +1-603-862-0188.
E-mail address: Stephen.Boles@unh.edu (S.H. Boles).

0034-4257/$ - see front matter © 2004 Elsevier Inc. All rights reserved.
doi:10.1016/j.rse.2004.01.016

A number of vegetation indices have been developed and used for monitoring vegetation structure and function, as well as land cover classification at large spatial scales. The Normalized Difference Vegetation Index (NDVI, Eq. (1)), which uses spectral information from the red and near infrared bands, is the most widely used. NDVI has served as the input data for various satellite-based land cover mapping activities (Defries & Townshend, 1994; Loveland et al., 2000). The shortwave infrared (SWIR) band is sensitive to vegetation cover, leaf moisture and soil moisture (Tucker, 1980), and a combination of the NIR and SWIR bands has the potential for retrieving canopy water content (Ceccato et al., 2002a,b). The Land Surface Water Index (LSWI, Eq. (2)) is calculated using NIR and SWIR reflectance values (Jürgens, 1997; Xiao et al., 2002b). Recently, LSWI has been used together with NDVI as input to land cover mapping efforts (Xiao et al., 2002b), with the expectation that the increased amount of spectral information provided from LSWI would improve the discrimination of vegetation types. It is known that NDVI has several limitations, including sensitivity to both atmospheric conditions (Xiao et al., 2003) and the soil background, and a tendency to saturate at closed vegetation canopies with large leaf area index values. To account for these limitations, the Enhanced Vegetation Index (EVI, Eq. (3)) was proposed, which directly adjusts the reflectance in the red spectral band as a function of the reflectance in the blue band (Huete et al., 1997; Liu & Huete, 1995):

$$\mathrm{NDVI} = (\rho_{\mathrm{nir}} - \rho_{\mathrm{red}})/(\rho_{\mathrm{nir}} + \rho_{\mathrm{red}}) \quad (1)$$

$$\mathrm{LSWI} = (\rho_{\mathrm{nir}} - \rho_{\mathrm{swir}})/(\rho_{\mathrm{nir}} + \rho_{\mathrm{swir}}) \quad (2)$$

$$\mathrm{EVI} = 2.5 \times \frac{\rho_{\mathrm{nir}} - \rho_{\mathrm{red}}}{\rho_{\mathrm{nir}} + 6 \times \rho_{\mathrm{red}} - 7.5 \times \rho_{\mathrm{blue}} + 1} \quad (3)$$

where ρ_{blue}, ρ_{red}, ρ_{nir}, and ρ_{swir} represent the surface reflectance values of blue, red, NIR, and SWIR bands, respectively.

In the evolution of land cover product generation, spectral input data have become increasingly tailored for land cover analyses. There is a need to assess the potential of using both EVI and LSWI for generating improved land cover classifications that take advantage of a much greater portion of the electromagnetic spectrum than previous NDVI-based products.

In this study, we explore the utility of multi-temporal VGT data for the mapping of land cover in Temperate East Asia (TEA). Our objectives were threefold: (1) to document the land cover of TEA using VGT data acquired in 2000; (2) to perform a validation of the land cover map using products derived from fine-resolution imagery; and (3) to analyze the seasonal dynamics of the various land cover types. This study outlines the potential for using VGT data to monitor the seasonal and inter-annual ecosystem dynamics in TEA. Such a regional level product can greatly improve the estimation of carbon and greenhouse gas fluxes in very dynamic and changing landscapes.

1.1. Study area

TEA is characterized by diverse land cover types, ranging from productive agricultural lands (e.g., North China Plain) to some of the most barren landscapes on Earth (e.g., Taklimakan and Gobi Deserts). The northern portion of TEA is covered by boreal forest and taiga, primarily dominated by larch and pine species. One of the most extensive temperate steppe grasslands in the world exists in the middle of the region. Land cover variability in TEA is strongly influenced by two factors: the monsoon climate system and elevation. The monsoon circulation creates a strong seasonality in precipitation availability, where the majority of annual precipitation falls in the critical growing season months. The amount and spatial distribution of the annual monsoon precipitation is con-

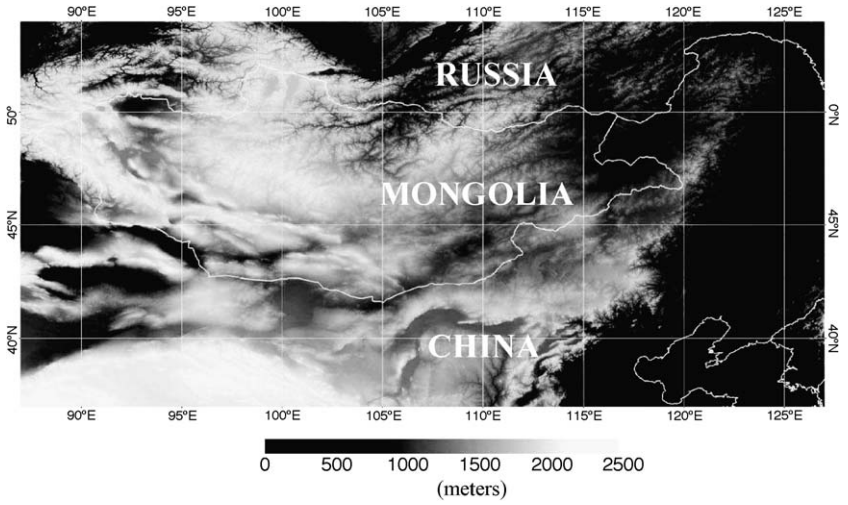

Fig. 1. An elevation map of TEA with national boundaries shown. The elevation product is the Global Land One-Kilometer Base Elevation dataset (http://www.ngdc.noaa.gov).

trolled by several moisture sources and prevailing winds (Xue, 1996). Elevation exerts a large influence on the land cover distribution of TEA because several sizable mountain ranges are located within the region, and much of the region is situated on plateaus with an average elevation well over 1000 m (Fig. 1).

While much of TEA remains remote and inaccessible, the area has experienced increased human and natural activities that have significantly altered the structure and function of the constituent ecosystems. Forests have become increasingly fragmented due to harvesting and agricultural encroachment (Wang et al., 2001), while natural wildfires cause landscape-level changes on an annual basis (Kasischke & Bruhwiler, 2002). Grasslands in TEA have been subjected to a range of anthropogenic activities, including cropland conversion and livestock grazing, which leads to overgrazing and desertification. Such changes can significantly alter the carbon dynamics of terrestrial ecosystems. It has been suggested that a large carbon sink is located in northern Asia (Bousquet et al., 1999). While the role of forests in this Northern Hemisphere carbon sink has been documented (Schimel et al., 2001), grasslands play a significant but poorly recognized role in the global carbon cycle (Scurlock & Hall, 1998). Grassland soil carbon stocks (where the vast majority of grassland carbon is stored) have been estimated at 10–30% of global soil carbon (Anderson, 1991; Eswaran et al., 1993).

2. Data and methods

2.1. VEGETATION image data and pre-processing

The VGT instrument has four spectral bands: blue (B0; $\lambda = 430–470$ nm), red (B2; $\lambda = 610–680$ nm), near infrared (B3; $\lambda = 780–890$ nm), and short-wave infrared (SWIR; $\lambda = 1580–1750$ nm), where λ represents the wavelength in each band. These are equivalent to Landsat Thematic Mapper (TM) bands 1, 3, 4, and 5, respectively. The blue band is primarily used for atmospheric correction. The SWIR band is sensitive to soil and vegetation moisture content, and can improve the discrimination of vegetation and other land cover types. With a swath width of 2250 km, VGT provides daily coverage of the globe at 1-km spatial resolution. Unlike scanner sensors (e.g., AVHRR), the VGT instrument uses linear-array technology and thus produces high-quality imagery at coarse resolution with greatly reduced distortion. VGT-S10 (10-day synthesis product) data were used in this analysis. This data is atmospherically corrected for ozone, aerosols and water vapor (Rahman & Dedieu, 1994). There are three 10-day composites for each month: days 1–10, 11–20, and 21 to the last day of a month. VGT-S10 data are generated by selecting the pixels that have the maximum NDVI values within a 10-day period. This approach helps to minimize the effect of cloud cover and variability in atmospheric optical depth. We downloaded year 2000 VGT-S10 data (http://free.vgt.vito.be) and generated a subset of composites for the TEA study area (37–54°N, 87–127°E). Both EVI and LSWI were calculated for each of the VGT-S10 products.

Although the maximum NDVI compositing procedure eliminates most cloudy pixels, some VGT-S10 products contain residual cloud contamination. We designed a simple approach (Xiao et al., 2003) to fill vegetation index values where the VGT Quality Assurance flags indicated cloudy pixels existed in the time series. Let $X(i,j,k)$ be the vegetation index value for pixel (i,j) and composite k (varying from 1 to 36 periods in a year). For a cloudy pixel in a 10-day composite k, $X(i,j,k)$, we first selected a three-point time-series filter, $X(i,j,k-1)$, $X(i,j,k)$, $X(i,j,k+1)$ and used values of non-cloudy pixels in this window to correct cloudy pixels. If both $X(i,j,k-1)$ and $X(i,j,k+1)$ pixels were cloud-free, we calculated the average of $X(i,j,k-1)$ and $X(i,j,k+1)$ and used the average value to replace $X(i,j,k)$. If only one pixel (either $X(i,j,k-1)$ or $X(i,j,k+1)$) was cloud-free, we used that pixel to replace $X(i,j,k)$. If the algorithm did not succeed in a three-point filter, we then extended to a five-point time-series filter, $X(i,j,k-2)$, $X(i,j,k-1)$, $X(i,j,k)$, $X(i,j,k+1)$, $X(i,j,k+2)$, using the same procedure as the three-point filter.

2.2. Classification and interpretation

There are two general approaches for land cover classification: per-pixel binary (0 or 1) and sub-pixel unmixing (percentage fractional cover within a pixel). The per-pixel binary approach is the most widely used method, including the International Geosphere-Biosphere Programme (IGBP) DISCover dataset (Loveland et al., 2000) and the GLC2000 dataset (http://www.gvm.jrc.it/glc2000/defaultGLC2000.htm). In this study, we explored the potential and limitations of the per-pixel binary approach using coarse-resolution VGT data and fine-resolution land cover products derived from Landsat images. An unsupervised classification procedure (ISODATA) was used for image classification (ENVI version 3.6), as it allows for the identification of all the important spectral groupings without initially knowing which are thematically significant (Cihlar et al., 1998). EVI and LSWI bands from March 1–10, 2000 to November 21–30, 2000 (a total of 54 bands) were used as input to the iterative ISODATA clustering algorithm. One hundred spectral clusters were generated with the following parameters: convergence threshold (95%), maximum number of merge pairs (2), minimum class standard deviation (1), minimum number of pixels in a class (100), and maximum number of iterations (10). Clusters containing mixed classes were separately reclassified in order to further extract individual classes.

Interpretation of spectral clusters into land cover types is to some degree dependent upon the land cover classification scheme. We felt that it was necessary to develop a more detailed land cover classification scheme, as opposed to using an existing generalized global legend (e.g., IGBP

DISCover). Temperate East Asia contains one of the world's largest temperate grasslands; these grasslands vary in composition from lush meadow vegetation to sparse desert steppe. It was our goal to discriminate the major grassland types that exist in the area (meadow, meadow steppe, typical steppe, desert steppe), and this could not be accomplished using the IGBP DISCover classes. Our land cover classification scheme, VGT-TEA, contains five classes of woody vegetation, six classes of grassland, two classes that contain cropland, and five classes of barren or sparsely vegetated land. Descriptions of these classes and their main vegetation components are provided in Table 1.

To aid in the interpretation and labeling of the spectral clusters, a number of ancillary data sets were used. Both the IGBP DISCover dataset (Loveland et al., 2000) and the Temperate East Asia Landcover (TEAL) dataset (Ojima et al., unpublished) were derived from 1-km 1992/1993 AVHRR data. The 1:4,000,000 Map of Rangeland Resources in China (CAS/SPC, 1996) provided information on the spatial extent of the major grassland categories in China.

Table 1
Descriptions and dominant vegetation components (Gao & Yu, 1998) of land cover classes within the *VGT-TEA* product

VGT-TEA class	Class description	Dominant components
Cropland	Land dedicated to the production of crops	N.A.
Cropland/natural vegetation	A mosaic of cropland and natural vegetation; no one component comprises more than 60% of the landscape	N.A.
Evergreen needleleaf forest	Dominated by evergreen needleleaf trees with a percent canopy cover greater than 60% and height exceeding 2 m	*Pinus*, *Picea*, and *Abies*
Deciduous broadleaf forest	Dominated by deciduous broadleaf trees with a percent canopy cover greater than 60% and height exceeding 2 m	*Quercus*, *Betula*, *Acer*, and *Populus*
Mixed forest	Dominated by mixed tree types with a percent canopy cover greater than 60% and height exceeding 2 m	*Pinus*, *Quercus*, *Betula*, and *Larix*
Deciduous needleleaf woodland	Dominated by deciduous needleleaf vegetation with a percent canopy cover less than 60%	*Larix sibirica*, *L. gmelini*
Mixed woodland	Dominated by mixed woody vegetation with a percent canopy cover less than 60%	*Pinus*, *Populus*, *Salix*
Shrubland/grassland	A mosaic of herbaceous and woody vegetation less than 2 m in height	*Quercus*, *Betula*, *Salix* (shrubs), *Stipa cleistogenes*, *Cleistogenes gramineae* (herbaceous)
Meadow/meadow steppe	Land covered with meadow or meadow steppe herbaceous plants and less than 10% woody vegetation cover	*Stipa baicalensis*, *Filifolium sibiricum*
Meadow steppe/typical steppe	Land covered with meadow steppe or typical steppe herbaceous plants and less than 10% woody vegetation cover	Combination of meadow steppe and typical steppe components
Typical steppe	Land covered with typical steppe herbaceous plants and less than 10% woody vegetation cover	*Aneurolepidium chinense*, *Stipa grandis*, *S. krylovii*
Desert steppe/typical steppe	Land covered with typical steppe or desert steppe herbaceous plants and less than 10% woody vegetation cover	Combination of typical steppe and desert steppe components
Desert steppe	Land covered with desert steppe herbaceous plants and less than 10% woody vegetation cover	*Stipa krylovii*, *S. breviflora*, *S. gobica*, *S. pennata*, *Cleistogenes soongorica*, *Allium polyrrhizum*
Desert steppe/desert	A mosaic of desert steppe herbaceous plants and exposed soil, sand, rocks or snow; less than 10% woody vegetation	*Stipa krylovii*, *S. breviflora*, *S. gobica*, *S. pennata*, *Cleistogenes soongorica*, *Allium polyrrhizum*
Desert	Areas of exposed soil, sand, rocks, or snow that never have more than 10% vegetated cover during any time of the year.	N.A.
Sparse vegetation	Vegetation cover (woody or herbaceous) of 10–30%	*Haloxylon ammodendron*, *Artemisia salsoloides*, *Anabasis brevifolia*
Tundra	Treeless ecosystems due to latitude or altitude. Vegetation consists primarily of grasses, sedges, small herbs, shrubs, lichen, and mosses.	Mosaic-shrubs, herbs, sedges, grasses, mosses, algae, lichens
Urban	Covered by buildings and other human-made structures	N.A.
Water/ice	Permanent water, ice, and snow	N.A.

The China National Land Cover Dataset (NLCD; described in detail in Section 2.3) was derived from Landsat Enhanced Thematic Mapper (ETM+) images acquired in 1999 and 2000. Since vegetation distribution is related to elevation gradients in the study area, the Global Land One-Kilometer Base Elevation dataset was obtained from the NOAA National Geophysical Data Center (http://www.ngdc.noaa.gov/) and subset to the study area (Fig. 1) and used as an aid for interpretation and labeling of the spectral clusters.

2.3. Accuracy assessment

Accuracy assessment of coarse-resolution land cover products is a critical and challenging task, as these maps can overestimate or underestimate cover types due to the fragmentation and sub-pixel proportion of each cover type (Achard et al., 2001). As an alternative approach to field surveys, fine-resolution images and derived land cover maps have been used for validation of coarse-resolution thematic maps (Scepan, 1999; Scepan et al., 1999). In this study, validation was performed in China and selected regions of Mongolia, as we had detailed datasets derived from fine-resolution Landsat data to support analysis in these areas (Fig. 2).

Recently, the National Land Cover Project (supported by the Chinese Academy of Sciences) completed the analysis of Landsat 7 ETM+ images acquired in 1999 and 2000 for China. Hundreds of ETM+ images were geo-referenced and ortho-rectified, using field-collected ground control points and fine-resolution digital elevation models. A classification system of 25 land cover types was used in the project. Visual interpretation of ETM+ images was conducted to generate a thematic map of land use and land cover in China at a scale of 1:100,000. The resultant vector National Land Cover Dataset (NLCD-1999/2000) was converted into a gridded database at 1-km resolution. The unique feature of this 25-layer gridded 1-km database is that it still captures all of the land cover information at the 1:100,000 scale by calculating percent fractional cover within a 1-km pixel for individual land cover types. The NLCD dataset was used in previous characterizations of China land cover (Frolking et al., 2002; Xiao et al., 2002b) and, in this analysis, it was used to validate VGT-TEA within the Chinese portion of TEA. One important issue that must be addressed when using one satellite-derived dataset for validation of another is consistent definition of land cover classes. At the detailed land cover class level, such as the individual forest or woodland types, there were inconsistent cover type definitions between NLCD and VGT-TEA. For example, NLCD defines forest as a canopy cover greater than 30%, while VGT-TEA adopts the IGBP DISCover definition of forest (greater than 60% canopy cover). This discrepancy in land cover definitions has been addressed by the aggregation of individual classes to very broad general land cover types (Table 2).

For validation of the Mongolian portion of TEA, land cover classifications from five Landsat TM images acquired in the early 1990s (Fig. 2) were used. The 30-m classification maps were aggregated to 1-km pixel size, such that each pixel represented percent fractional cover for individual land cover types. Because of a lack of available fine-resolution reference data in 1999/2000 for Mongolia, it was necessary to use the TM classifications even though the dates did not coincide with VGT-TEA. However, we are confident that the different imaging times of the TM and VGT products had minor impacts on the validation exercise for two main reasons: (a) generalized land cover classes were used (Table 2), likely accounting for potential spectral differences due to inter-annual variation in vegetative cover; and (b) the Mongolian portion of TEA has experienced less

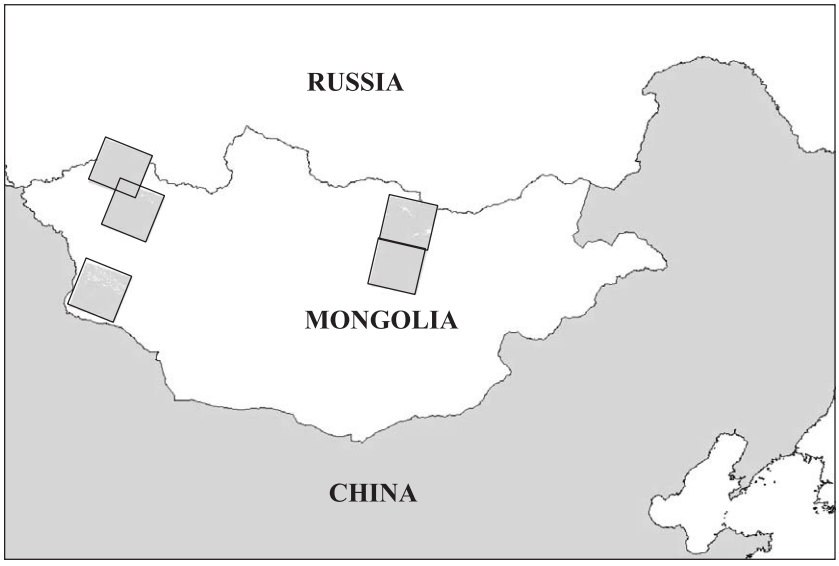

Fig. 2. Location of Thematic Mapper data (grey areas) that was used for validation of the VGT-TEA product in China and Mongolia.

Table 2
Land cover classes in the VGT-TEA product (left column) with codes used to identify the classes in Figs. 3–5

VGT-TEA land cover	Aggregated land cover	Area (1000 km^2)
Cropland	cropland	562
Cropland/natural vegetation	cropland/natural vegetation	384
Evergreen needleleaf forest (ENF)	woody vegetation	159
Deciduous broadleaf forest (DBF)	woody vegetation	109
Mixed forest (MXF)	woody vegetation	417
Deciduous needleleaf woodland (DNW)	woody vegetation	176
Mixed woodland (MXW)	woody vegetation	378
Shrubland/grassland	shrubland/grassland	153
Meadow steppe/meadow (M Stp/M)	grassland	141
Typical steppe/meadow steppe (T Stp/M Stp)	grassland	322
Typical steppe (T Stp)	grassland	785
Typical steppe/desert steppe (T Stp/D Stp)	grassland	119
Desert steppe (D Stp)	grassland	380
Desert steppe/desert (D Stp/D)	sparsely vegetated	40
Desert	sparsely vegetated	472
Sparse vegetation	sparsely vegetated	915
Tundra	sparsely vegetated	135
Urban	sparsely vegetated	4
Water/ice	water	72

'Aggregated land cover' indicates the general land cover category to which each class was assigned in the validation exercises. The area column represents total area for the VGT-TEA class within TEA.

intensive changes in land cover than other areas. Table 2 outlines the class aggregations that were used so that the three classifications (VGT-TEA, NLCD, Mongolian TM) could be compared.

3. Results

3.1. VGT classification map of Temperate East Asia (VGT-TEA)

VGT-TEA contains five classes of woody vegetation, five classes of grassland, four classes of barren or sparsely vegetated land, two classes of mixed land cover (cropland/natural vegetation mosaic, shrubland/grassland), and single classes of cropland, tundra, and water (Fig. 3). A distinct gradient of land cover types exists within TEA, as is evident in Fig. 3. The great deserts of northwestern China and southern Mongolia are a harsh and sparsely vegetated landscape that accounts for approximately one-quarter of the TEA land area. The temperate steppe ecosystem, which surrounds the vast desert, accounts for approximately one-third of the TEA land area. Within the temperate steppe ecosystem a gradient of grassland types exists, gradually changing from desert steppe to typical steppe to meadow in the northern and eastern directions. Woody vegetation (forests, woodlands, shrublands) accounts for just over one-quarter of the TEA land area, and is primarily situated in southern Russia and northeastern China. Cropland occupies a large swath of land in the North China Plain and Liaohe River valley, and represents the largest component of the remaining land area in TEA.

3.2. Comparison of land cover type area estimates

Aggregation of classes to the most general land cover types allows for a comparison of land cover totals derived from different satellite sensors. While the VGT and IGBP products were available for the entire study area, the Landsat-derived NLCD product was only available for China, and thus class area summaries were performed in the China potion of TEA only (Table 3). Some obvious differences exist between the class summaries derived from coarse-resolution (VGT-TEA, IGBP) and fine-resolution (NLCD) input data. The coarse-resolution products estimate much smaller land cover components of both the water and built-up classes. These two land covers often exist at a scale that is much finer than the 1-km resolution of the VGT and AVHRR sensors, and thus are suppressed by spatial aggregation and not identified. Compared to the NLCD product, VGT-TEA underestimates both woody vegetation and grassland cover if only pure pixels (pixels classified as one land cover type) are considered. However, VGT-TEA contains two mixed classes (cropland/natural vegetation, shrubland/grassland) that are partially composed of woody vegetation and grassland. As part of the validation procedure, the frequency distributions of both VGT-TEA mixed classes were calculated in reference to the fractional cover of each NLCD land cover type in China. Using this method of class decomposition, the two mixed classes (combined) were determined to have the following compositions: grassland (44%), cropland (21%), woody vegetation (20%), barren/sparsely vegetated (7%), and other (8%). If these proportions are added to the pure pixel total, many of the class areas of VGT-TEA are similar to the NLCD product (Table 4).

In addition to the comparisons of remote sensing products using aggregated land cover classes, a more detailed analysis of grassland types can be made between VGT-TEA and the Map of Rangeland Resources in China (CAS/SPC, 1996). Compared to the Map of Rangeland Resources, VGT-TEA (pure pixels) underestimates the total grassland area, yet several of the major types (typical steppe, desert steppe, desert) are similar in area. The main discrepancy between the Map of Rangeland Resources and VGT-TEA occurs in the meadow/meadow steppe category (Table 5), which is greatly underestimated in the VGT-TEA product. Some of this discrepancy can be accounted for by VGT-TEA mixed classes (meadow steppe/typical steppe, shrub-

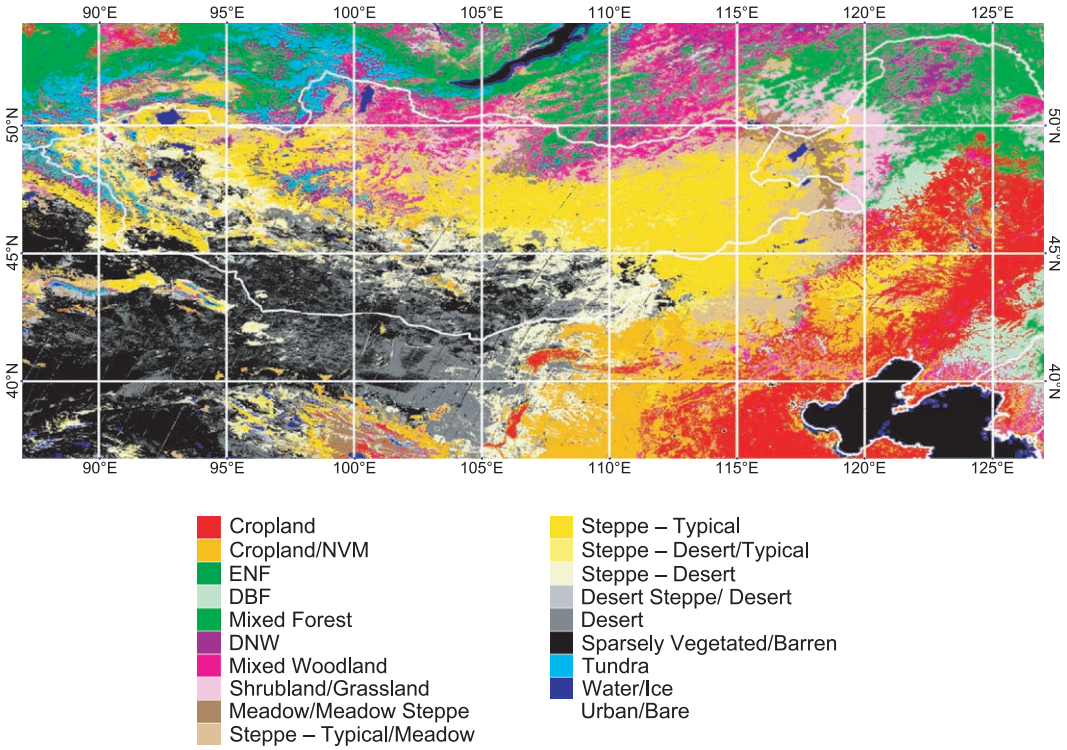

Fig. 3. VGT-TEA land cover classification derived from year 2000 VGT data; class codes are defined in Table 2.

land/grassland, cropland/natural vegetation) that likely contain a proportion of meadow/meadow steppe vegetation.

3.3. Accuracy assessment of VGT-TEA classification

3.3.1. China

The NLCD dataset contains percentage fractions of individual land cover types within 1-km pixels as determined from fine-resolution Thematic Mapper data. Within the Chinese portion of TEA, each aggregated land cover class from VGT-TEA was overlaid with the NLCD product in a geographical information system (ArcINFO version 8.0). This provides quantitative information (Table 6) on the contribution of individual NLCD land cover components for: (a) each of the aggregated land cover classes in VGT-TEA (cropland, woody vegetation, grassland, sparsely vegetated) and (b) two mixed classes in VGT-TEA (cropland/natural vegetation mosaic, shrubland/grassland). Results of the land cover decomposition of the two VGT-TEA mixed classes are presented in Section 3.2 and Table 6.

The accuracy of the aggregated VGT-TEA classes can be defined as the percentage of each class that corresponds to the same aggregated land cover in the NLCD product. Of the four major aggregated land cover classes (cropland, woody vegetation, grassland, sparsely vegetated), the sparsely vegetated category had the highest accuracy at 80.5%. This category was most often misclassified as grassland, likely due to the expansive transition zones that

Table 3
Estimates of aggregated land cover area (1000 km^2) for the China portion of the TEA study area, as estimated from various remote sensing products

Land cover	VGT-TEA	NLCD	IGBP
Woody vegetation	351[a]	437	957[b]
Grassland	698[a]	909	620[c]
Sparsely vegetated	1019[a]	1057	730
Cropland	464	421	451
Cropland/NVM	320	NA	276
Shrub/grassland	66	NA	NA

VGT-TEA and IGBP products are per-pixel 1-km classifications, while NLCD estimates were derived from 1999/2000 Thematic Mapper data.
[a] Components of this aggregated class can be found in Table 1.
[b] Includes all IGBP forest, shrub, and woody savanna classes.
[c] Includes IGBP grassland and savanna classes.

Table 4
Estimates of aggregated land cover area (1000 km^2) for the China portion of the TEA study area

Land cover	VGT-TEA	NLCD
Woody vegetation	429[a]	437
Grassland	880[a]	909
Sparsely vegetated	1048[a]	1063
Cropland	548	421

VGT estimates include proportions of the two mixed classes (cropland/NVM, shrubland/grassland) that were decomposed by comparing to the NLCD fractional composition of that area (Table 6).
[a] Components of this aggregated class can be found in Table 2.

Table 5
Estimates of grassland types (1000 km^2) for the China portion of the TEA study area, as estimated from the VGT-TEA classification and the Map of Rangeland Resources of China (CAS/SPC, 1996)

Grassland type	VGT-TEA	Rangeland map of China
Desert	333[a]	373[a]
Desert steppe	184	187[a]
Typical steppe/desert steppe	32	78
Typical steppe	294	312
Meadow/meadow steppe	74	419[a]
Meadow steppe/typical steppe	131	NA
Shrubland/grassland	69	NA
Cropland/NVM	343	NA

[a] Indicates that this grassland type was generated from the aggregation of more detailed types.

contain noticeable components of both sparsely vegetated land and grassland. Less than 1% of the VGT-TEA sparsely vegetated category corresponded to NLCD cropland or woody vegetation land cover, likely due to: (a) contrasting spectral signatures between the land cover classes and (b) geographically distinct areas of these land cover types that aid in their discrimination. The VGT-TEA grassland category had a detection accuracy of 60.2% and was most often misclassified as sparsely vegetated land, likely due to the expansive transition zones that occur between these two land cover types. The VGT-TEA woody vegetation category had the second highest detection accuracy (72.4%) and was largely misclassified as either grassland or cropland. The VGT-TEA cropland category had the lowest detection accuracy (54.5%) compared to the NLCD product. A contributing factor to this lower accuracy may be a more heterogenous nature of the cropland category due to small field sizes and the presence of agriculture-related infrastructure (buildings, roads, ponds, etc.) in close proximity to the fields. Because the NLCD product was derived from Thematic Mapper imagery, a greater proportion of the smaller cropland areas could be identified than with the 1-km spatial resolution VGT imagery.

Table 7
Total estimates of aggregated land cover area (km^2) from the five Mongolian validation areas

Land cover	VGT-TEA	TM	IGBP
Woody vegetation	30,454[a]	30,368	60,092[b]
Grassland	97,298[a]	49,983	74,988[c]
Sparsely vegetated	26,318[a]	75,737	17,595
Cropland	218	1697	2661
Water	5847	6082	6065
Crop/NVM	191	NA	2384
Shrubland/grassland	3564	NA	NA

[a] Components of this aggregated class can be found in Table 2.
[b] Includes all IGBP forest, shrub, and woody savanna classes.
[c] Includes IGBP grassland and savanna classes.

3.3.2. Mongolia

To validate the Mongolian portion of VGT-TEA, five TM scenes from the early 1990s were used with classes aggregated to match the VGT-TEA product. Table 7 is a summary of the areas of each of the aggregated classes for all of the TM scenes. The area estimates of both water and woody vegetation from the two products were very close. Cropland was underestimated by VGT-TEA, yet this cover type represented a very small proportion of the five areas used for validation. The grassland and sparsely vegetated land cover types are characterized by large discrepancies in area as estimated by VGT-TEA and the TM classifications (Table 7). However, it is interesting to note that the sum of both grassland and sparsely vegetated land are very close. One possibility is that this discrepancy between grassland and sparsely vegetated land is due to interannual variations of climate and land cover type as opposed to actual permanent land cover change. Much of Mongolia's population still maintains the sustainable pastoral lifestyle, and the landscape has not been subject to the same anthropogenic pressure as exists in Inner Mongolia of China. Interannual variation in the climate of the steppe grasslands of TEA is well documented (Fernandez-Gimenez & Allen-Diaz, 1999; Lee et al., 2002; Xiao et al., 1995). Significant

Table 6
Results of the validation of the China portion of the study area

		NLCD (Landsat) land cover (1000 km^2)						
		Cropland	Woody vegetation	Grassland	Sparsely vegetated	Water	Urban	Total area (VGT-TEA)
VGT-TEA land cover (1000 km^2)	Cropland	253	67	81	18	13	32	464
	Woody Vegetation	30	254	48	14	3	2	351
	Grassland	49	31	420	176	13	9	698
	Sparsely Vegetated	4	6	178	820	6	5	1019
	Cropland/NVM	79	56	147	25	6	7	320
	Shrubland/Grassland	5	22	35	4	0	0	66
	Total area (NLCD)	420	436	909	1057	41	55	

Each aggregated land cover class from VGT-TEA was overlaid with the NLCD (Landsat) product in a GIS (ArcInfo 8.0). This exercise revealed the distribution of actual land cover components for each aggregated land cover class in VGT-TEA. Rows represent the aggregated VGT-TEA land cover classes, while columns represent the aggregated NLCD (Landsat) land cover classes. Note that the mixed land cover classes in VGT-TEA (cropland/NVM, shrubland/grassland) do not have identical NLCD classes; however, they are included so that the distribution of actual land cover in these classes can be shown. Components of the aggregated VGT-TEA land cover classes are shown in Table 2.

variations in steppe vegetation in the amount of biomass (Fernandez-Gimenez & Allen-Diaz, 1999; Xiao et al., 1995) and vegetative cover (Fernandez-Gimenez & Allen-Diaz, 1999) have been documented between years due to differing levels of precipitation. However, analysis of long-term climate records did not reveal significant differences in temperature or precipitation between the times of imaging for the Landsat in early 1990s and VGT-TEA products in 2000. Another potential reason for the discrepancy between grassland and sparsely vegetated area estimates is different land cover class definitions and aggregations employed in the Landsat image classifications. For example, the Mongolian TM products contained only two grassland classes (meadow and steppe) that were aggregated for validation purposes. VGT-TEA contains five categories of grassland that were aggregated (Table 2) for comparison to the Mongolian TM products. If all VGT-TEA land cover classes that contain desert steppe (typical steppe/desert steppe, desert steppe) were included in the 'sparsely vegetated' aggregated category, VGT-TEA area estimates of grassland and sparsely vegetated land cover (approx. 76,000 and 54,000 km^2, respectively) would be much closer to the Landsat estimates.

3.4. Seasonal dynamics of vegetation indices

Summary statistics of the LSWI and EVI (Figs. 4 and 5, respectively) time series for all of the woody vegetation and grassland cover types were calculated in order to characterize seasonal dynamics of vegetation indices. It is likely that the sharp decrease of LSWI in the spring and sharp increase of LSWI in the fall can be attributed to snowmelt and snow accumulation, respectively. There is much greater variation in the timing of snowmelt and snow accumulation for the woody vegetation cover types (Fig. 4a) than the grassland (Fig. 4b). The LSWI time series is characterized by distinct 'troughs' in the spring and fall seasons that indicate the transitional periods between a snow-dominated landscape and a foliage-dominated landscape. During these trough periods, the spectral signal is dominated by non-photosynthetic vegetation and the soil background, resulting in the lowest LSWI values of the year. By defining the timing and

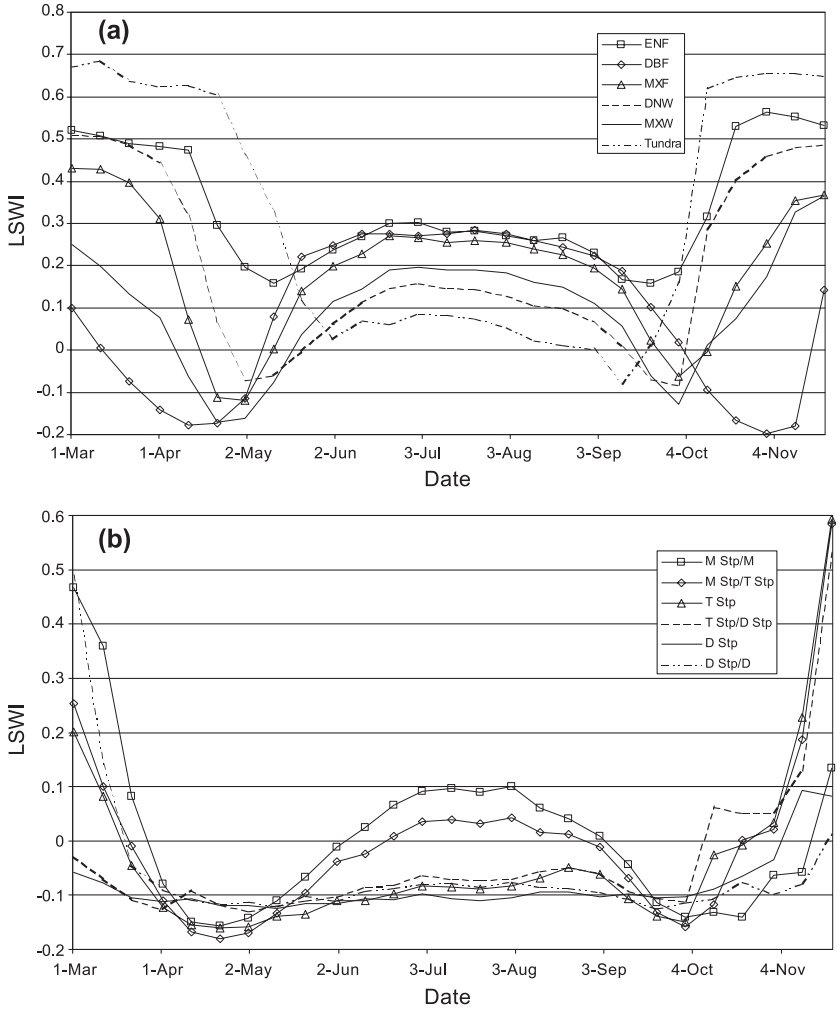

Fig. 4. Seasonal dynamics of LSWI values from March 1 to November 30, 2000 for (a) the woody vegetation cover types and (b) grassland cover types, within TEA; class codes are defined in Table 2.

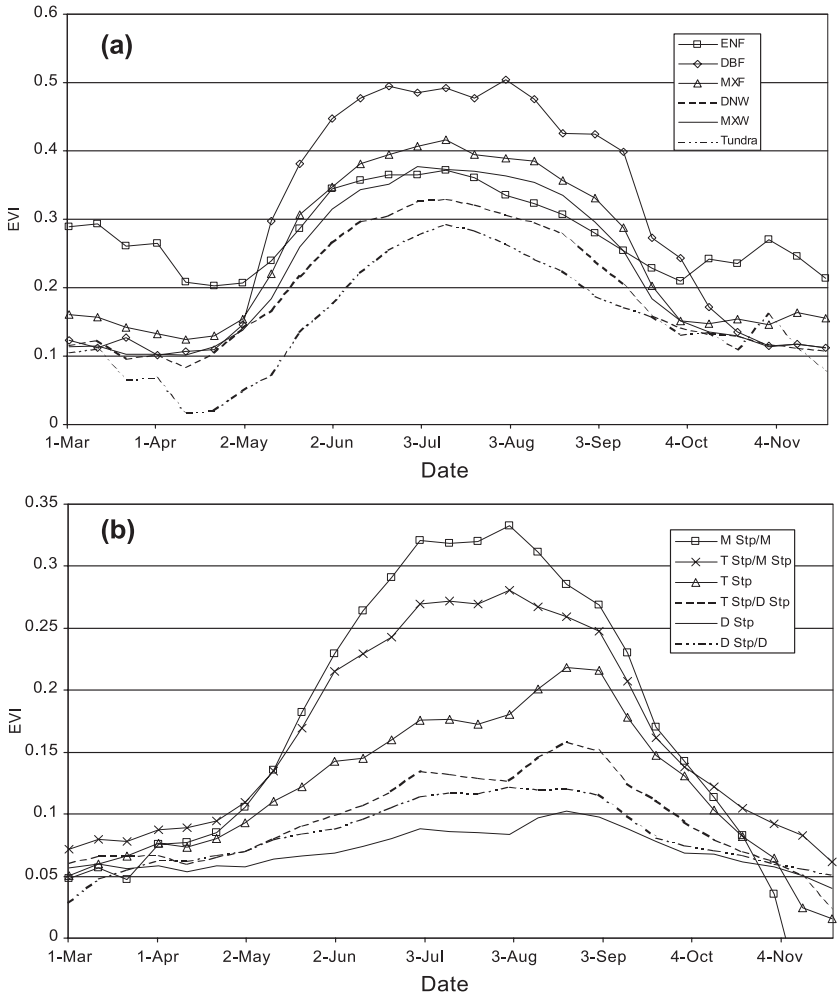

Fig. 5. Seasonal dynamics of EVI values from March 1 to November 30, 2000 for (a) the woody vegetation cover types and (b) grassland cover types, within TEA; class codes are defined in Table 2.

length of the plant growing season with the LSWI 'troughs', it is evident that there is a great degree of variation in growing season length amongst woody vegetation cover types (Fig. 4a), with the growing season for deciduous broadleaf forest being several weeks longer than other kinds of woody vegetation. The majority of the deciduous broadleaf forest in our study area was located in Northeastern China. These forests are a mix of the southern reaches of the boreal forest and the northern extent of the temperate mixed hardwood forest. All of the other forest/woody categories in our study (evergreen needleleaf, deciduous needleleaf, mixed) contained a considerable portion of coniferous vegetation. These classes were located in the northern portion of the study area (boreal ecosystem) or at the grassland/boreal transition zone. The reason for the longer growing season in the deciduous broadleaf category is likely a function of both warmer temperature and increased moisture availability in northeastern China. Woody vegetation in TEA is controlled by both temperature/elevation and precipitation regimes, as opposed to the grassland areas that are uniformly driven by the summer monsoon precipitation only. The seasonal dynamics of the precipitation-driven grassland cover types (Fig. 4b) exhibit a growing season from late April–early May to late September. Grassland cover types also exhibit very little variation in foliar moisture content during the peak growing season. While it is possible to spectrally distinguish the areas that contain meadow/meadow steppe vegetation from other grassland types, all of the classes that contain only typical/desert steppe are indistinguishable in terms of foliar moisture. This is likely a result of the strong soil background signal that is present in these grassland types.

The EVI time series for woody vegetation (Fig. 5a) reveals considerable differences in EVI values during the peak growing season (July and August), ranging from approximately 0.35 (evergreen needleleaf forest) to 0.5 (deciduous broadleaf forest). This is indicative of the greater chlorophyll content of the broadleaf canopy. This strong contrast in EVI values between broadleaf and needleleaf forests, which has also been observed using MODIS data (Huete et al., 2002), could be useful in the discrimination and mapping of forest types. For woody

land cover types containing deciduous or mixed vegetation, the EVI values at the beginning and end of the growing season (as determined from the LSWI time series) are approximately 0.15. This threshold value could potentially be used as an indicator of deciduous growing season length from EVI data, although this will need further testing in other areas of woody vegetation. The EVI time series for grassland (Fig. 5b) was slightly more effective at discriminating between grassland types and featured a greater dynamic range of values during the peak growing season than the LSWI time series (Fig. 5b). There was an expected decrease of EVI values from meadow vegetation to typical steppe to desert steppe, based on the structure of the grasses and the canopy cover. Interestingly, the peak values of both EVI and LSWI differ among the grassland types, with the meadow/meadow steppe categories achieving their maximum index values in mid-July, and all other categories (typical and desert steppes) achieving their maximum index values in mid-August.

4. Discussion and conclusions

The results of this study have demonstrated the potential of improved vegetation indices (EVI and LSWI) for land cover classification in Temperate East Asia. Seasonal dynamics of vegetation indices is correlated to vegetation phenology and widely used in land cover classification at large spatial scales. Accurate measurements of vegetation phenology for various vegetation types are required to improve our understanding of the interannual variability of carbon exchange in terrestrial ecosystems for use in production efficiency models (Zhang et al., 2003). Information on the timing and length of the plant growing season is needed in the estimation of gross primary production (photosynthesis) and can be inferred from the seasonal dynamics of vegetation indices. While satellite sensors may be limited in their ability to detect some traditional phenological events (e.g., budding, flowering), they are capable of detecting broad landscape-level changes that are descriptive of the ecosystem as a whole (Tieszen et al., 1997). With the introduction of a new generation of moderate resolution optical sensors (VGT, MODIS) in recent years, there is the opportunity to utilize a greater number of spectral bands in analyses of vegetation. This study highlights the utility of using *both* EVI and LSWI seasonal time series in analyses of land cover phenology. Previously, AVHRR-derived NDVI data have been used to define the length of temperate forest growing seasons, using NDVI threshold values ranging from 0.25 (Myneni et al., 1998) to 0.45 (Jenkins et al., 2002). However, for deciduous broadleaf forests, seasonal EVI curves are more symmetrical about the peak of the growing season (Huete et al., 2002) when compared to NDVI. In addition, the sensitivity to canopy leaf structure results in strong contrasts of EVI values between needleleaf and broadleaf forests (Huete et al., 2002) that may aid in the mapping and discrimination of forest types. In a previous analysis of Northeast China forests (Xiao et al., 2002b), we suggested that additional information regarding vegetation phenology can be extracted from the seasonal dynamics of LSWI. In this analysis, we suggest that the LSWI time series can be used to define the growing season of different vegetation types as the period between the spring and fall troughs (Fig. 4a). This between-trough period indicates the existence of canopy moisture. The use of the LSWI time series to define the vegetation growing seasons resulted in phenological patterns that would be expected, such as a much longer growing season for deciduous broadleaf forest than tundra.

Because grasslands cover a significant proportion of the Earth's surface and play a pivotal role in the global carbon cycle, there have been several previous remote sensing analyses of grassland phenology (Davidson & Csillag, 2003; Reed et al., 1994; Ricotta et al., 2003; Tieszen et al., 1997). These studies utilized time series of NDVI composites (10-day or bi-monthly temporal resolution) from the AVHRR sensor, for the purpose of analyzing differences in net primary productivity between C_3 and C_4 grasslands in North America. The distribution of C_3 and C_4 grasses could be determined by differences in satellite-derived phenological indicators, including growing season onset and cessation. Our analysis highlights the potential utility of both LSWI and EVI seasonal time series for the delineation of grassland growing season, and to a lesser extent grassland type mapping. As with forest, the LSWI time series can be used to define the growing season of grassland types as the period between the spring and fall troughs (Fig. 4b). Due to the limited dynamic range of values for the grassland types, LSWI could only be used to discriminate between the grasslands that contained meadow/meadow steppe and those that did not. However, the slightly larger dynamic range of EVI values during the peak growing season (Fig. 5b) may allow for more detailed discrimination of grassland types (meadow steppe, typical steppe, desert steppe). The discrimination of grassland types from the seasonal dynamics of spectral indices is of critical importance due to the high interannual variability in land cover and biomass that exists within the temperate grasslands of TEA. The interannual variability is due to both biotic (e.g., grazing, disease, insects) and abiotic factors (drought, extreme temperatures) and can have a significant impact on the area occupied by each grassland type each year.

It is evident that TEA is an area of significance in regards to the global carbon cycle due to the expanses of forests, woodlands, and grasslands. Because of the variability in land cover (especially grassland) that occurs in TEA on an annual basis, frequent monitoring is necessary to provide timely and accurate input to production efficiency models. Our results show that the seasonal dynamics of multitemporal VGT spectral indices can be used to discriminate vegetation type and the duration of the growing season for various types of vegetation. This analysis would benefit

from validation efforts of the vegetation phenology patterns (field observations of spring green-up and fall senescence) determined from the spectral indices and further large-scale validation of the land cover map in Mongolia and Siberia. The development of VGT-TEA has shown that moderate resolution satellite data can be used to: (a) develop reasonably accurate land cover maps in a region of high land cover diversity and (b) monitor the seasonal dynamics of vegetation and use these patterns to discriminate vegetation types.

References

Achard, F., Eva, H., & Mayaux, P. (2001). Tropical forest mapping from coarse spatial resolution satellite data: Production and accuracy assessment issues. *International Journal of Remote Sensing*, *22*, 2741–2762.

Anderson, J. M. (1991). The effects of climate change on decomposition processes in grassland and coniferous forests. *Ecological Applications*, *1*, 326–347.

Bartalev, S. A., Belward, A. S., Erchov, D. V., & Isaev, A. S. (2003). A new SPOT-4 VEGETATION derived land cover map of Northern Eurasia. *International Journal of Remote Sensing*, *24*, 1977–1982.

Bousquet, P., Ciais, P., Peylin, P., Ramonet, M., & Monfray, P. (1999). Inverse modeling of annual atmospheric CO2 sources and sinks: I. Method and control inversion. *Journal of Geophysical Research*, *104*, 26161–26178.

CAS/SPC, Chinese Academy of Science and State Planning Commission (1996). *Map of rangeland resources of China*. Beijing: Science Press, Sponsored by: Ministry of Agriculture.

Ceccato, P., Flasse, S., & Gregoire, J. -M. (2002a). Designing a spectral index to estimate vegetation water content from remote sensing data: Part 2. Validation and applications. *Remote Sensing of Environment*, *82*, 198–207.

Ceccato, P., Gobron, N., Flasse, S., Pinty, B., & Tarantola, S. (2002b). Designing a spectral index to estimate vegetation water content from remote sensing data: Part 1. Theoretical approach. *Remote Sensing of Environment*, *82*, 188–197.

Cihlar, J., Xiao, Q., Chen, J., Beaubien, J., Fung, K., & Latifovic, R. (1998). Classification by progressive generalization: A new automated methodology for remote sensing multichannel data. *International Journal of Remote Sensing*, *19*, 2685–2704.

Davidson, A., & Csillag, F. (2003). A comparison of three approaches for predicting C_4 species cover of northern mixed grass prarie. *Remote Sensing of Environment*, *86*, 70–82.

Defries, R., & Townshend, J. (1994). NDVI-derived land classifications at a global scale. *International Journal of Remote Sensing*, *17*, 3567–3586.

Eswaran, H., van den Berg, E., & Reich, P. (1993). Organic carbon in soils of the world. *Soil Science Society of America Journal*, *57*, 192–194.

Fernandez-Gimenez, M. E., & Allen-Diaz, B. (1999). Testing a non-equilibrium model of rangeland vegetation dynamics in Mongolia. *Journal of Applied Ecology*, *36*, 871–885. doi: 10.1029/2001GBO01425.

Frolking, S., Qiu, J., Boles, S., Xiao, X., Liu, J., Zhuang, Y., Li, C., & Qin, X. (2002). Combining remote sensing and ground census data to develop new maps of the distribution of rice agriculture in China. *Global Biogeochemical Cycles*, *16* (art. no. 1091).

Gao, Q., & Yu, M. (1998). A model of regional vegetation dynamics and its application to the study of Northeast China Transect (NECT) responses to global change. *Global Biogeochemical Cycles*, *12*, 329–344.

Huete, A., Didan, K., Miura, T., Rodriguez, E. P., Gao, X., & Ferreira, L. G. (2002). Overview of the radiometric and biophysical performance of the MODIS vegetation indices. *Remote Sensing of Environment*, *83*, 195–213.

Huete, A. R., Liu, H. Q., Batchily, K., & van Leeuwen, W. (1997). A comparison of vegetation indices over a global set of TM images for EOS-MODIS. *Remote Sensing of Environment*, *59*, 440–451.

Jenkins, J. P., Braswell, B. H., Frolking, S. E., & Aber, J. A. (2002). Predicting spatial and interannual patterns of temperate forest springtime phenology in the eastern U.S.. *Geophysical Research Letters*, *29* (art. no. 2201). doi: 10.1029/2001GLO14008.

Jürgens, C. (1997). The modified normalized difference vegetation index (mNDVI)-a new index to determine frost damages in agriculture based on Landsat TM data. *International Journal of Remote Sensing*, *18*, 3583–3594.

Kasischke, E. S., & Bruhwiler, L. P. (2002). Emissions of carbon dioxide, carbon monoxide, and methane from boreal forest fires in 1998. *Journal of Geophysical Research*, *108* (art. No. 8146). doi: 10.1029/2001JDO00461.

Lee, R., Yu, F., Price, K. P., Ellis, J., & Shi, P. (2002). Evaluating vegetation phenological patterns in Inner Mongolia using NDVI time-series analysis. *International Journal of Remote Sensing*, *23*, 2505–2512.

Liu, H. Q., & Huete, A. R. (1995). A feedback based modification of the NDVI to minimize canopy background and atmospheric noise. *IEEE Transactions on Geoscience and Remote Sensing*, *33*, 457–465.

Loveland, T. R., Reed, B. C., Brown, J. F., Ohlen, D. O., Zhu, Z., Yang, L., & Merchant, J. W. (2000). Development of a global land cover characteristics database and IGBP DISCover from 1-km AVHRR data. *International Journal of Remote Sensing*, *6*, 1303–1330.

Myneni, R. B., Tucker, C. J., Asrar, G., & Keeling, C. D. (1998). Interannual variations in satellite-sensed vegetation index data from 1981 to 1991. *Journal of Geophysical Research*, *103*, 6145–6160.

Rahman, H., & Dedieu, G. (1994). SMAC: A simplified method for atmospheric correction of satellite measurements in the solar spectrum. *International Journal of Remote Sensing*, *15*, 123–143.

Reed, B. C., Brown, J. F., VanderZee, D., Loveland, T. R., Merchant, J. W., & Ohlen, D. O. (1994). Measuring phenological variability from satellite imagery. *Journal of Vegetation Science*, *5*, 703–714.

Ricotta, C., Reed, B. C., & Tieszen, L. T. (2003). The role of C_3 and C_4 grasses to interannual variability in remotely sensed ecosystem performance over the US Great Plains. *Interntional Journal of Remote Sensing*, *24*, 4421–4431.

Scepan, J. (1999). Thematic validation of high-resolution global land-cover data sets. *Photogrammetric Engineering and Remote Sensing*, *65*, 1051–1060.

Scepan, J., Menz, G., & Hansen, M. C. (1999). The DIScover validation image interpretation process. *Photogrammetric Engineering and Remote Sensing*, *65*, 1075–1081.

Schimel, D. S., House, J. I., Hibbard, K. A., Bousqet, P., Ciais, P., Peylin, P., Braswell, B. H., Apps, M. J., Baker, D., Bondeau, A., Canadell, J., Churkina, G., Cramer, W., Denning, A. S., Field, C. B., Friedlingstein, P., Goodale, C., Heimann, M., Houghton, R. A., Melillo, J. M., Moore III, B., Murdiyarso, D., Noble, I., Pacala, S. W., Prentice, I. C., Raupach, M. R., Rayner, P. J., Scholes, R. J., Steffen, W. L., & Wirth, C. (2001). Recent patterns and mechanisms of carbon exchange by terrestrial ecosystems. *Nature*, *414*, 169–172.

Scurlock, J. M. O., & Hall, D. O. (1998). The global carbon sink: A grassland perspective. *Global Change Biology*, *4*, 229–233.

Tieszen, L. L., Reed, B. C., Bliss, N. B., Wylie, B. K., & DeJong, D. D. (1997). NDVI, C_3 and C_4 production, and distributions in Great Plains grassland land cover classes. *Ecological Applications*, *7*, 59–78.

Tucker, C. J. (1980). Remote sensing of leaf water content in the near-infrared. *Remote Sensing of Environment*, *10*, 23–32.

Wang, X., Feng, Z., & Ouyang, Z. (2001). The impact of human disturbance on vegetative carbon storage in forest ecosystems in China. *Forest Ecology and Management*, *148*, 117–123.

Xiao, X., Boles, S., Frolking, S., Salas, W., Moore III, B., Li, C., He, L., & Zhao, R. (2002a). Landscape-scale characterization of cropland in China using Vegetation and Landsat TM images. *International Journal of Remote Sensing*, *23*, 3579–3594.

Xiao, X., Boles, S., Liu, J., Zhuang, D., & Liu, M. (2002b). Character-

ization of forest types in northeastern China, using multi-temporal SPOT-4 VEGETATION sensor data. *Remote Sensing of Environment*, *82, 335–348.*

Xiao, X., Braswell, B., Zhang, Q., Boles, S., Frolking, S., & Moore, B. (2003). Sensitivity of vegetation indices to atmospheric aerosols: Continental-scale observations in Northern Asia. *Remote Sensing of Environment*, *84*, 385–392.

Xiao, X., Wang, Y., Jiang, S., Ojima, D. S., & Bonham, C. D. (1995). Interannual variation in the climate and aboveground biomass of *Leymus chinense* steppe and *Stipa grandis* steppe in the Xilin river basin, Inner Mongolia, China. *Journal of Arid Environments*, *31*, 283–299.

Xue, Y. (1996). The impact of desertification in the Mongolian and the Inner Mongolian Grassland on the regional climate. *Journal of Climate*, *9*, 2173–2189.

Zhang, X., Friedl, M. A., Schaaf, C. B., Strahler, A. H., Hodges, J. C. F., Gao, F., Reed, B. C., & Huete, A. (2003). Monitoring vegetation phenology using MODIS. *Remote Sensing of Environment*, *84*, 471–547.